

Structural phase transition in Bi_2Se_3 under high pressure

Zhenhai Yu¹, Lin Wang^{1,2,8*}, Qingyang Hu^{1,8}, Jinggeng Zhao³, Shuai Yan⁴, Ke Yang⁴, Matthew Suchomel⁵, Stanislav Sinogeikin⁶, Genda Gu⁷ & Ho-kwang Mao^{1,6,8}

¹Center for High Pressure Science and Technology Advanced Research, Shanghai, 201203, People's Republic of China,

²State Key Laboratory of Superhard Materials, Jilin University, Changchun 130012, People's Republic of China,

³Natural Science Research Center, Academy of Fundamental and Interdisciplinary Sciences, Harbin Institute of Technology, Harbin 150080, People's Republic of China,

⁴Shanghai Institute of Applied Physics, Chinese Academy of Sciences, Shanghai 201203, People's Republic of China,

⁵X-ray Science Division, Advanced Photon Source, Argonne National Laboratory, Argonne, Illinois 60439, United States of America,

⁶High Pressure Collaborative Access Team, Geophysical Laboratory, Carnegie Institution of Washington, Argonne, Illinois 60439, United States of America,

⁷Condensed Matter Physics and Materials Science Department, Brookhaven National Laboratory, Upton, New York 11973, United States of America,

⁸Geophysical Laboratory, Carnegie Institution of Washington, Washington, DC 20015, United States of America,

* Corresponding author, Tel: 1(630)252-6763 (office), Fax 1(630)252-9303.

E-mail address: wanglin@hpstar.ac.cn, or lwang@carnegiescience.edu (Lin Wang).

Raman spectroscopy and angle dispersive X-ray diffraction (XRD) experiments of bismuth selenide (Bi_2Se_3) have been carried out to pressures of 35.6 and 81.2 GPa, respectively, to explore its pressure-induced phase transformation. The experiments indicate that a progressive structural evolution from ambient rhombohedra phase (Space group (SG): $R\bar{3}m$) to monoclinic phase (SG: $C2/m$) and eventually to a high pressure body-centered tetragonal phase (SG: $I4/mmm$). Evidenced by our XRD data up to 81.2 GPa, Bi_2Se_3 crystallizes into body centered tetragonal structure rather than the recently reported disordered body centered cubic (BCC) phase. Furthermore, first principles theoretical calculations favor the viewpoint that the $I4/mmm$ phase Bi_2Se_3 can be stabilized under high pressure (> 30 GPa). Remarkably, the Raman spectra of Bi_2Se_3 from this work (two independent Runs) are still Raman active up to ~ 35 GPa. It is worthy to note that the disordered BCC phase at 27.8 GPa is not observed in our work. The remarkable difference in atomic radii of Bi and Se in Bi_2Se_3 may be responsible for rationalizing why Bi_2Se_3 shows different structural behavior than those of isocompounds Bi_2Te_3 and Sb_2Te_3 .

Topological insulators (TIs) are electronic materials that have a bulk band gap like the ordinary insulators, but feature conducting states on their surface. Besides the importance of theoretical investigation in condensed matter physics, TIs have various applications in spintronics^{1,2}, quantum computation^{3,4} and thermoelectric energy conversion^{5,6}. It is of fundamental significance to understand the crystal structure of TIs under controlled external conditions. The A_2B_3 ($A = \text{Sb, Bi}$; $B = \text{Se, Te}$) series TIs such as Bi_2Te_3 , Sb_2Te_3 , and Bi_2Se_3 belong to a class of three dimensional topological insulators which possess exotic gapless surface states^{7,8}. Bi_2Se_3 is an ideal candidate for studying room temperature topological insulating behavior as it has a topologically nontrivial band gap of 0.3 eV, much larger than the room temperature energy scale⁹.

Bi_2Se_3 , Bi_2Te_3 , and Sb_2Te_3 are among the most interested compounds of three dimensional TIs^{10,11}. Although these compounds were under extensive studies in 1950s and 1960s as excellent thermoelectric materials, some basic physical properties still remain unexplored. External pressure is well known to provide a powerful method to tune the atom arrangement and the consequential properties of the materials. In situ X-Ray diffraction (XRD) investigation on two kinds of TIs (Bi_2Te_3 and Sb_2Te_3) under high pressure showed that both of them exhibited the same sequence of transformation with step-increasing coordination number of Bi atoms, where the crystal structure transforms from $R-3m$ (CN = 6) \rightarrow $C2/m$ (CN = 7) \rightarrow $C2/c$ (CN = 8) \rightarrow $Im-3m$ (CN = 8)^{12,13}. Bi_2Se_3 is an isostructural compound to Bi_2Te_3 and Sb_2Te_3 , so it is naturally to speculate that Bi_2Se_3 would follow the same sequence of

transformation under high pressure. The structural variations of Bi_2Se_3 have drawn many experimental interests. Angular dispersive powder XRD and Raman spectrum measurement on Bi_2Se_3 was carried out using a Merrill-Bassett diamond anvil cell (DAC) by Vilaplana *et al.*¹⁴, whose results evidenced a pressure-induced structural phase transition of $R-3m$ (CN = 6) \rightarrow $C2/m$ (CN = 7) \rightarrow $C2/c$ (CN = 8) \rightarrow $Im-3m$ (CN = 8) structures at 10, 20 and 28 GPa, respectively. Since the Raman spectra of Bi_2Se_3 were inactive above 27.8 GPa, the authors reasoned Bi_2Se_3 crystallizing into disordered BCC structure above that pressure. At the same time, other high pressure XRD works on Bi_2Se_3 have been performed by other research groups¹⁵⁻¹⁷. However, the assignment of high pressure phase was controversial from different literatures as shown in Fig. 1 (a). Several selected literally reported crystallographic structures of Bi_2Se_3 under different external conditions were illustrated in Fig. 1 (b). To the best of our knowledge, at least seven crystallographic models for Bi_2Se_3 were reported previously.

Given the above mentioned confused experimental and calculation results on the polymorphism of Bi_2Se_3 under high pressure, our work is motivated to deal with two major issues: (1) The ambiguity around 10 GPa lies in the resemblance in $C2/m$ and $C2/c$ phase of Bi_2Se_3 since space group of $C2/c$ is a subgroup of $C2/m$. (2) differentiating $I4/mmm$ and $Im-3m$ phase of Bi_2Se_3 depends on whether we could identify weak diffraction peaks over low angle. As mentioned above, due to the lack of systematic work, the crystallographic polymorphism under high pressure is still unclear. To the aforementioned issues, we have carried out high pressure synchrotron

XRD studies on Bi_2Se_3 under high pressure aiming to investigate the pressure-induced structural transformation in Bi_2Se_3 . Furthermore, Raman spectra measurements on Bi_2Se_3 under high pressure were also performed with different pressure-transmitting medium (PTM) to promote the clarification of polymorphism in Bi_2Se_3 . At last the structural stability of $I4/mmm$ phase of Bi_2Se_3 was also investigated by theoretical calculations.

Results

To begin with, the phase quality of the samples in the present study was confirmed by high resolution synchrotron XRD technique as shown in Fig. S1. Selected angular dispersive XRD patterns recorded from ambient pressure up to 81.2 GPa of this work are shown in Fig. 2. No splitting or occurrence of new diffraction peaks are observed below 9.4 GPa. Therefore, the indexing of diffraction peaks, lattice constant refining and peak fitting processes during ambient pressure to 9.4 GPa were based on the space group $R-3m$. The Rietveld refined diffraction patterns of $R-3m$ phase at selected pressures are depicted in Fig. 3(a). The angular dispersive XRD pattern of Bi_2Se_3 is readily fitted by the rhombohedral phase model with additional Au peaks as the pressure marker. The pressure dependence of the axial ratio (c/a) for $R-3m$ phase of Bi_2Se_3 is reported in Fig. S3. Electronic topological transition (ETT) or Lifshitz transition is defined as variation in the topology of the Fermi energy surface. This transition is induced by compression or alloying which is able to tune the electronic structure of the material¹⁸. Bi_2Te_3 , Sb_2Te_3 and Bi_2Se_3 crystallize into $R-3m$ crystal

structure at ambient conditions. It was observed that the ETT in α -Bi₂Te₃ leads to a pronounced change in the c/a ratio at ~ 3 GPa¹⁹. The similar variation in c/a ratio was also observed in Bi₂Se₃ from the present experimental XRD results. Our present measurement indicate that pressure induced ETT in Bi₂Se₃ occurred ~ 3 GPa. The pressure-induced ETT in Bi₂Se₃ from this work is different from Ref. 14 (see supplementary information).

Although the pressure-induced structural phase transition in Bi₂Se₃ around 10 GPa had been intensively investigated during the past years, an ambiguity in space group ($C2/m$ or $C2/c$) assignment centered around the slide plane or mirror plane of the high pressure phase still exists. A more detailed analysis on the crystallographic information for Bi₂Se₃ with $C2/m$ phase with different assignments on Wyckoff position for Bi and Se atoms is provided in Fig. 1 (b). The significant difference of XRD pattern of Bi₂Se₃ around 14 GPa between nonhydrostatic and quasihydrostatic pressure conditions is that the diffraction peak among d -spacing of 2.7939 Å ($2\theta = 8.346^\circ$) and 2.6019 Å ($2\theta = 8.963^\circ$) under quasihydrostatic pressure is one merged diffraction peak¹⁶, while this merged diffraction peak split into two separate diffraction groups under nonhydrostatic conditions as shown in Fig. S4. Our experimental XRD patterns of Bi₂Se₃ is compared with the calculated XRD patterns with $C2/c$ (CN = 8) and $C2/m$ (CN = 7) space groups at 14 GPa (Fig. S4). The results from comprehensive analysis selects the $C2/m$ (CN = 7) as the more favorable structure for Bi₂Se₃ at this pressure. A typical Rietveld refinement of $C2/m$ phase of Bi₂Se₃ is shown in Fig. 3 (b).

The author in Ref. [14] commented that Bi_2Se_3 follow the same sequence of structural transformation as observed in Bi_2Te_3 and Sb_2Te_3 isostructures. Given that Bi_2Se_3 forms a disordered BCC structure above 25 GPa, no Raman active modes can be detected. However, in this work, Raman modes were still observable in Bi_2Se_3 even at 35 GPa. The detailed information will be discussed in the following Raman spectroscopy section.

The high quality of angle dispersive synchrotron XRD of Bi_2Se_3 in this study enable us to differentiate weak diffraction peaks located at lower angles. The angular dispersive XRD data can be unambiguously fitted into the space group of $I4/mmm$ for the best results. Therefore, we concluded that Bi_2Se_3 actually crystallizes into body centered tetragonal structure when it is pressurized above 30 and up to 81.2 GPa. The Rietveld refinement of the body centered tetragonal structure is shown in Fig. 3 (c). Another series of duplicate high pressure XRD measurement was performed at BL15U1 beamline of Shanghai Synchrotron Radiation Facility (SSRF). The results shown in Fig. S2 confirms our conclusion.

In order to verify our speculation on the crystallographic structural phase transition sequence of Bi_2Se_3 under high pressure, Raman scattering spectroscopy, which is a more sensitive technique in investigating vibrational, rotational, and other low-frequency modes of materials, was employed to characterize the pressure-induced structural phase transition. At ambient conditions, Bi_2Se_3 crystallizes into a rhombohedral structure with space group $R-3m$, which contains five atoms in a primitive unit cell. Therefore, there are four Raman-active modes ($2A_{1g} + 2E_g$) and

four IR-active modes ($2A_{2u} + 2E_u$). A 4:1 methanol-ethanol mixture was used as PTM in Raman experiment, several selected typical Raman spectra consisting Stokes contribution in Run 1 were shown in Fig. 4. The Raman spectrum for $R-3m$ phase of Bi_2Se_3 was located at the lower panel of Fig. 4. The present measured Raman spectrum of $R-3m$ phase of Bi_2Se_3 agrees nicely with the experimental results in Ref. 14.

According to the group theory analysis and the literature reported results²⁰⁻²², the Raman peaks located ~ 72.4 , ~ 133.2 and 174.3 cm^{-1} are identified to the A_{1g}^1 , E_g^2 and A_{1g}^2 vibrational modes, respectively. As the pressure increasing, we found from Fig. 4 that all the three Raman peaks shift to higher wavenumbers (blue shift). The Raman peaks representing the E_g^2 and A_{1g}^2 modes appears as single sharp peaks up to about 10 GPa. Those peaks are greatly broad beyond 10 GPa and new Raman peaks appear, indicating structural changes have occurred. In line with the XRD experiment, this is attributed to the structural phase transformation from hexagonal ($R-3m$) to monoclinic phase ($C2/m$). The onset on the structural phase transition is assigned around 10.1 GPa on the basis of Raman observation. Upon further compression, we observed that the Raman spectrum above ~ 28 GPa is unambiguously different from that of the $C2/m$ phase.. These results support our XRD assignment from which $C2/m$ phase of Bi_2Se_3 transformed to tetragonal phase ($I4/mmm$) above 28.1 GPa. Though the Raman peaks become more and more broaden as the pressure increasing. The Raman spectra of $I4/mmm$ phase of Bi_2Se_3 were still discernable up to 35.2 GPa.

The Raman spectrum has almost disappeared at 27.8 GPa in Ref. 14, and the author

suggested that Bi_2Se_3 transformed to a new phase which is Raman inactive. Remarkably, although Raman spectrum becomes broaden and turns into a low signal noise ratio stat, the Raman spectrum does not disappear until to the highest pressure (35.6 GPa, Run 1) in all of experimental runs, Therefore, we suggest that Bi_2Se_3 did not reach to the disordered BCC structure around 35.6 GPa.

Corresponding to the present nonhydrostatic XRD measurement, the Raman scattering experiment here was also performed without PTM. Furthermore, the similarities and differences of Raman spectra for Bi_2Se_3 under different pressure conditions could be obtained. The Raman spectra of Bi_2Se_3 under various pressures without PTM were shown in Fig. S6. Comparing to the results at hydrostatic conditions in Fig. 4, we note that the profile of Raman spectra is mostly the same as what we have collected with pressure medium, which is 4:1 methanol-ethanol mixture. The Raman spectra of Bi_2Se_3 in the present pressure scope reproduce our high pressure XRD analysis.

In order to confirm the mechanical stability of $I4/mmm$ phase of Bi_2Se_3 , we carried out phonon calculation under the framework of density functional theoretical (DFT). The results are listed in an evolution of increasing pressure (Fig. 5), where the compression of the system results in the blue shift of the all phonon mode frequencies, reproducing the experiments. Up to 100 GPa, no negative modes are seen in the phonon dispersion curves, indicating the structure is mechanically stable. The proved stability from phonon analysis is consistent with our XRD and Raman experiment.

Discussion

The high-pressure phase of Bi_2Se_3 , transformed from $C2/m$ phase has three debating candidates, which are $Im-3m$ ¹⁴, $C2/m$ (CN= 9/10)¹⁵ and $I4/mmm$ ¹⁶. To clarify the polymorphism in Bi_2Se_3 , we enumerate the experimental XRD data around 30 GPa from this work and calculated XRD with three candidate space groups reported in the literatures. In Fig. S5, the simulated XRD with $C2/m$ (CN = 9/10) and $Im-3m$ could not match the experimental XRD data collected from this work.

The A_2B_3 (A = Sb, Bi; B = Se, Te) series compounds such as Bi_2Te_3 , Sb_2Te_3 , and Bi_2Se_3 were reported to exhibit topological properties^{7,11}. Therefore it is nature to check if the isocompound Sb_2Se_3 would exhibit the same properties. Very recently, Sb_2Se_3 is reported to transforms into topological insulator from non-topological state above ~ 2 GPa and form a disordered BCC structure above 51 GPa²³. At ambient conditions, the radii of the Se, Te, Sb and Bi atoms are 1.15, 1.40, 1.45 and 1.60 Å, respectively²⁴, from which we could found that Bi and Se atoms possess the biggest atomic radii difference among the above mentioned four atoms. Therefore a certain pressure could not make these Bi and Se atoms resemble. The pressure-induced disordered substitution $Im-3m$ structure in Bi_2Te_3 , Sb_2Te_3 and Sb_2Se_3 was not observed in Bi_2Se_3 until to 81.2 GPa from this work.

The equation of state for Bi_2Se_3 is shown in Fig. 6. The unit cell volume for $R-3m$ phase obtained from this work matches literature results from Ref. 14 and 16, but exhibits smaller volume at same pressure than that in Ref. 15. This contradiction may be due to the different preparation techniques in synthesizing sample. Given the XRD data from this work and previous reported results, the pressure of phase transition in

Bi_2Se_3 was assigned to ~ 10 ($R-3m - C2/m$) and 25 ($C2/m - I4/mmm$) GPa, respectively. Although the polymorphism of Bi_2Se_3 under high pressure remain under debate, it is generally accepted that the pressure-induced structural phase transition in Bi_2Se_3 possess the feature of first order phase transition.

Pressure dependence c/a ratio of $I4/mmm$ phase for Bi_2Se_3 is plotted in the inset of Fig. 6. As shown in Fig. 1 (b). one lattice cell of the $I4/mmm$ phase contains ten Bi/Se atoms. The value of c/a ratio approaches 5.00 if $I4/mmm$ phase transformed to BCC phase. It can be seen from inset of Fig. 6 that the value of c/a ratio shows a dome-shaped pressure dependence. It reaches a maximum of 4.90 at around 60 GPa then it follows a decrease as the pressure increasing. The present pressure dependence of c/a ratio for $I4/mmm$ phase for Bi_2Se_3 was consistent with the foregoing XRD and Raman measurements.

In conclusion, a joint first-principles theoretical calculation and experimental measurement have been performed to investigate the pressure-induced structural phase transitions in Bi_2Se_3 . High pressure XRD results reveal two pressure-induced structural phase transitions in Bi_2Se_3 which did not follow the sequence of transformation in isostructural compounds Bi_2Te_3 and Sb_2Te_3 . The Raman spectra results rule out the previous hypothesis which Bi_2Se_3 transformed into a disordered BCC structure around 30 GPa. The present experimental XRD measurement and DFT calculation is consistent in structural stability of $I4/mmm$ phase under high pressure.

Materials & Methods

Crystal growth and preparation

The Bi₂Se₃ single crystals of this work were grown by a unidirectional solidification method with slow cool down. The single crystals were ground in a mortar in order to obtain a fine powder sample used in the following high resolution synchrotron XRD, high pressure angle dispersive XRD and Raman experiments.

High resolution synchrotron XRD

To begin with, the phase purity of sample (Bi₂Se₃) used in this work was confirmed by using high resolution synchrotron XRD measurement. High resolution synchrotron XRD data were collected using the powder diffractometer at 11 BM-B beamline of Advanced Photon Source at Argonne National Laboratory. The wavelength was fixed at 0.4124 Å. The wavelength was calibrated using Si 640c as a standard. The samples were finely ground and housed in glass capillaries that were continuously rotated during the measurements.

High pressure synchrotron angular dispersive XRD

High pressure synchrotron XRD were obtained using a symmetric diamond anvil cell with 200 μm culet diameter. A rectangle foil of rhenium was indented down to a thickness of 35 μm using the anvil face. A 60-μm gasket hole was made by drilling at the center of indentation in the foil. The powdered sample was put in the gasket hole without pressure medium. After the sample was pressed by the anvil, some gold powder was loaded on the flat of the sample to calculate the value of the pressure in the sample chamber²⁵. Angular dispersive powder XRD patterns were taken with a Mar3450 detector using synchrotron radiation beams monochromatized to a

wavelength of 0.4066 Å at 16 ID-B beamline of Advanced Photon Source at Argonne National Laboratory. An independent high pressure XRD experiment was performed at BL15U1 beamline at Shanghai Synchrotron Radiation Facility (SSRF) using a monochromatic beam of 0.6199 Å. The two-dimensional image plate patterns were integrated to one-dimensional pattern by using of Fit2D software package²⁶. The resulting diffraction patterns were fitted via Rietveld refinement through GSAS package²⁷.

Raman spectroscopy under high pressure condition

The Raman spectroscopy investigation on Bi₂Se₃ under high pressure was carried out using a commercial Renishaw Raman spectroscopy system in the backscattering configuration excited with a He/Ne laser ($\lambda = 632.8$ nm). The spectra resolution is as small as 1 cm⁻¹, and the lowest available frequency is 50 cm⁻¹. Two independent high-pressure Raman experiments were implemented on Bi₂Se₃. The methanol and ethanol mixture was using as PTM in Run 1, and no PTM was applied in Run 2.

Density functional calculation

In this study, the first-principles calculations²⁸⁻³⁰ were performed in the framework of density functional theory through Vienna *ab initio* simulation package³¹. The generalized gradient approximation under Perdew-Wang parameterization³² was implemented to describe the exchange correlation functions. The Projected-augmented wave potentials^{33,34} were used with 24 valence electrons for Bi (6s²6p³) and 8 for Se (4s²4p⁴). A plane-wave basis set with kinetic energy cut off of 300 eV was found sufficient to converge the total energy less than 10⁻⁶ eV and force

acting on each atom less than 0.01 eV/Å. One single Bi₂Se₃ unit cell (10 atoms, space group *I4/mmm*) is used for calculating electronic structures, where the Brillouin zone is sampled by a Monkhorst mesh³⁵ of 5×5×1 k-points, providing totally 9 irreducible k-points. A denser k-points (10×10×2) mesh was tested and the energy difference with the 5×5×1 mesh is less than the energy convergence criterion. Therefore the smaller mesh was used for all of our calculations. Hydrostatic pressure is applied by adding pulay stress to the diagonal elements of the stress tensor. At each pressure, the unit cell is fully optimized for atomic position, cell shape and cell volume.

We carried out supercell approach (2×2×1 supercell) within the finite displacement method for the phonon calculations³⁶. Force constants are calculated using Moore–Penrose pseudo-inverse by fitting symmetry reduced elements of force constants to the linear relations between atomic forces and atomic displacements by the Phonopy package³⁷.

Reference

1. Moore, J. E. The birth of topological insulators. *Nature* 464, 194–198 (2010).
2. Zayzev, O. V., Moore, J. E. & Louie, S. G. Spin Polarization and Transport of Surface States in the Topological Insulators Bi₂Se₃ and Bi₂Te₃ from First Principles, *Phys. Rev. Lett.* 105, 266806 (2010).
3. Fu, L. & Kane, C. L. Superconducting Proximity Effect and Majorana Fermions at the Surface of a Topological Insulator. *Phys. Rev. Lett.* 100, 096407 (2008).
4. Qi X. L. & Zhang, S. C. Topological insulators and superconductors. *Rev. Mod. Phys.* 83, 1057–1110 (2011).
5. Ghaemi, P., Mong, R. S. K. & Moore, J. E. In-Plane Transport and Enhanced Thermoelectric Performance in Thin Films of the Topological Insulators Bi₂Te₃ and Bi₂Se₃. *Phys. Rev. Lett.* 105, 166603 (2010).
6. Hinsche, N. F., Yavorsky, B. Y., Mertig, I. & Zahn, P. Influence of strain on anisotropic thermoelectric transport in Bi₂Te₃ and Sb₂Te₃. *Phys. Rev. B* 84, 165214. (2011).
7. Zhang, H. J. et al. Topological insulators in Bi₂Se₃, Bi₂Te₃ and Sb₂Te₃ with a single Dirac cone on the surface. *Nature Phys.* 5, 438–442 (2009).
8. Xia, Y. et al. Observation of a large-gap topological-insulator class with a single Dirac cone on the surface. *Nature Phys.* 5, 398–402 (2009).
9. Hasan, M.Z. & Kane, C. L. Colloquium: Topological insulators. *Rev. Mod. Phys.* 82 3045–3067. (2010).
10. Hsieh, D. et al. Observation of Time-Reversal-Protected Single-Dirac-Cone Topological-Insulator States in Bi₂Te₃ and Sb₂Te₃. *Phys. Rev. Lett.* 103, 146401 (2009).
11. Chen, Y. L. et al. Observation of Time-Reversal-Protected Single-Dirac-Cone Topological-Insulator States in Bi₂Te₃ and Sb₂Te₃. *Science* 325, 178–181 (2009).
12. Zhu, L. et al. Substitutional Alloy of Bi and Te at High Pressure. *Phys. Rev. Lett.* 106, 145501 (2011).
13. Zhao, J. G. et al. Pressure-Induced Disordered Substitution Alloy in Sb₂Te₃. *Inorg. Chem.* 50 11291–11293 (2011).
14. Vilaplana, R. et al. Structural and vibrational study of Bi₂Se₃ under high pressure. *Phys. Rev. B* 84, 184110 (2011).
15. Liu, G. T. et al. Stabilization of 9/10-Fold Structure in Bismuth Selenide at High Pressures. *J. Phys. Chem. C* 117, 10045–10050 (2013).
16. Zhao, J. G. et al. High-pressure phase transitions, amorphization, and crystallization behaviors in Bi₂Se₃. *J. Phys.: Condens. Matter* 25, 125602 (2013).
17. Kirshenbaum Kevin. et al. Pressure-Induced Unconventional Superconducting Phase in the Topological Insulator Bi₂Se₃. *Phys. Rev. Lett.* 111, 087001 (2013).
18. Struzhkin, V. V., Timofeev, Y. A., Hemley, R. J. & Mao, H. K., Superconducting T_c and Electron-Phonon Coupling in Nb to 132 GPa: Magnetic Susceptibility at Megabar Pressures. *Phys. Rev. Lett.* 79, 4262–4265 (1997).
19. Polian, A. et al. Two-dimensional pressure-induced electronic topological transition in Bi₂Te₃. *Phys. Rev. B* 83, 113106 (2011).
20. Zhang, J. et al. Raman Spectroscopy of Few-Quintuple Layer Topological Insulator Bi₂Se₃ Nanoplatelets. *Nano Lett.* 11, 2407–2414 (2011).
21. Rauh, H. et al. Generalized phonon density of states of the layer compounds Bi₂Se₃, Bi₂Te₃, Sb₂Te₃ and Bi₂(Te_{0.5}Se_{0.5})₃, (Bi_{0.5}Sb_{0.5})₂Te₃. *J. Phys. C Solid State Phys.* 14, 2705–2712 (1981).
22. Richter, W., & Becker, C. R. A Raman and far-infrared investigation of phonons in the rhombohedral V₂–VI₃ compounds Bi₂Te₃, Bi₂Se₃, Sb₂Te₃ and Bi₂(Te_{1–x}Se_x)₃ (0 < x < 1), (Bi_{1–y}Sb_y)₂Te₃ (0 < y < 1). *Phys. Status Solidi B* 84, 619–628 (1977).
23. Efthimiopoulos, I. et al. Sb₂Se₃ under pressure. *Sci. Rep.* 3, 2665 (2013).
24. Slater, J. C. Atomic Radii in Crystals. *J. Chem. Phys.* 41, 3199–3204 (1964).
25. Anderson, O.L., Isaak, D.G. & Yamamoto, S. Anharmonicity and the equation of state for gold, *J. Appl. Phys.* 65, 1534–1543 (1989).
26. Hammersley, A. P., Svensson, S. O., Hanfland, M., Fitch, A. N. & Hausermann, D. Two-dimensional detector software: From real detector to idealised image or two theta scan. *High Pressure Res.* 14, 235–248 (1996).
27. Toby, B. EXPGUI, a graphical user interface for GSAS. *J. Appl. Crystallogr.* 34, 210–213 (2001).

28. Vanderbilt, D. Soft self-consistent pseudopotentials in a generalized eigenvalue formalism, *Phys. Rev. B* 41, 7892–7895 (1990).
29. Gonze, X. First-principles responses of solids to atomic displacements and homogeneous electric fields: Implementation of a conjugate-gradient algorithm, *Phys. Rev. B* 55, 10337–10354 (1997).
30. Jaffe, J. E., Snyder, J. A., Lin, Z., Hess, A. C., LDA and GGA calculations for high-pressure phase transitions in ZnO and MgO, *Phys. Rev. B* 62, 1660–1665 (2000).
31. Kresse, G. & Furthmuller, J., Efficient iterative schemes for ab initio total-energy calculations using a plane-wave basis set, *Phys. Rev. B* 54, 11169–11186 (1996).
32. Perdew, J. P. & Wang, Y., Accurate and simple analytic representation of the electron-gas correlation energy, *Phys. Rev. B* 45, 13244–13249 (1992).
33. Blochl, P. E., Projector augmented-wave method, *Phys. Rev. B* 50, 17953–17979 (1994).
34. Kresse, G. & Joubert, D., From ultrasoft pseudopotentials to the projector augmented-wave method, *Phys. Rev. B* 59, 1758–1775 (1999).
35. Monkhorst, H. J. & Pack, J. D., Special points for Brillouin-zone integrations, *Phys. Rev. B* 13, 5188–5192 (1976).
36. Parlinski, K., Li, Z. Q. & Kawazoe, Y., First-Principles Determination of the Soft Mode in Cubic ZrO₂, *Phys. Rev. Lett.* 78, 4063–4066 (1997).
37. Togo, A., Oba, F. & Tanaka, I., First-principles calculations of the ferroelastic transition between rutile-type and CaCl₂-type SiO₂ at high pressures, *Phys. Rev. B* 78 134106 (2008).

Figure captions

Fig. 1 (a) Phase diagram of Bi_2Se_3 under room temperature with increasing pressure referenced from adapted literatures [14-17]. (b) Selected crystallographic structure models of Bi_2Se_3 under different external conditions.

Fig. 2 The selected angle dispersive XRD patterns of Bi_2Se_3 under various pressures at room temperature from ambient pressure up to 81.2 GPa. The diffraction peaks of Au were marked with dashed lines.

Fig. 3 Typical Rietveld refinement results of Bi_2Se_3 under (a) 4.6, (b) 14.1, and (c) 81.2 GPa.. The experimental and simulated data were symbolled with black solid sphere and red line. The solid short vertical lines show the positions of the allowed Bragg reflections for Bi_2Se_3 and Au. The difference between the observed and the fitted XRD patterns were shown with a line at the bottom of the diffraction peaks.

Fig. 4 Pressure dependence of Raman spectra of Bi_2Se_3 during compression using 4:1 methanol-ethanol mixture.

Fig. 5 Selected pressure dependence of phonon dispersion for $I4/mmm$ phase of Bi_2Se_3 .

Fig. 6. Pressure dependence of lattice volume for Bi_2Se_3 . Open symbol data were taken from Ref. 14, 15 and 16. Data from this work were marked with solid legend. Pressure dependence of c/a ratio of $I4/mmm$ phase for Bi_2Se_3 was shown in inset, where dashed lines were guide for eyes.

Figure 1 (a) and (b)

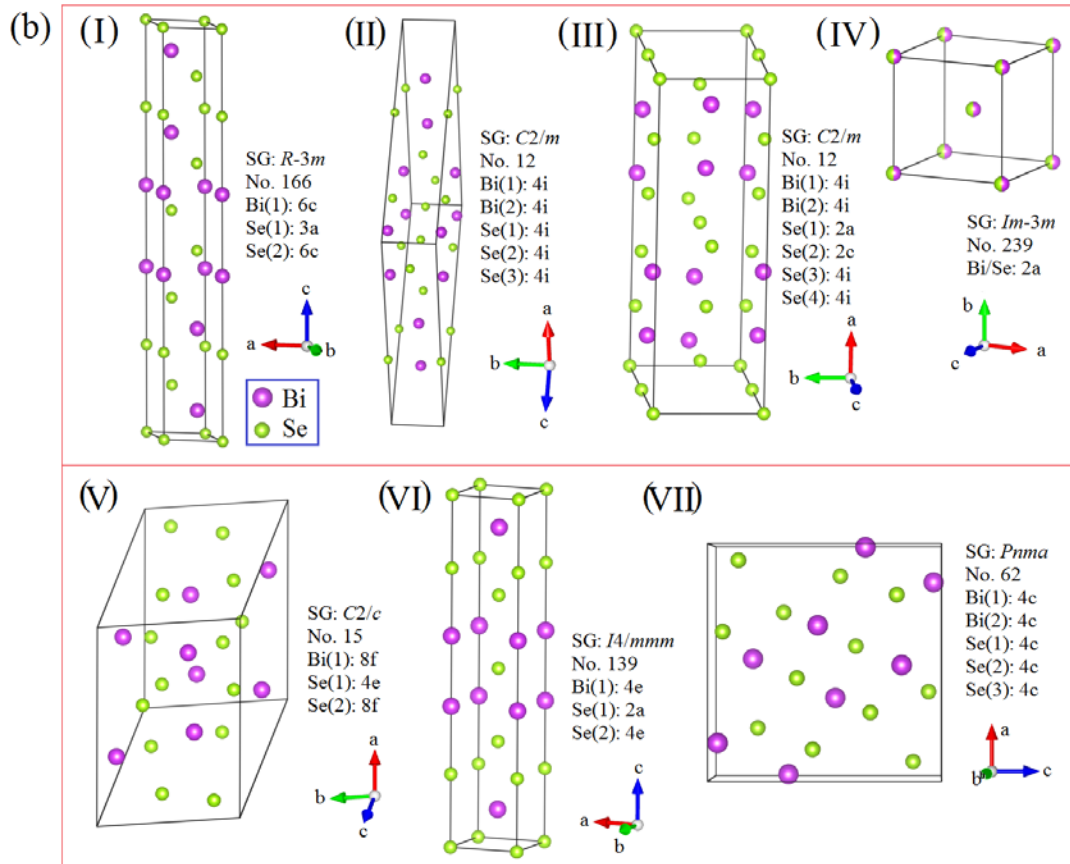
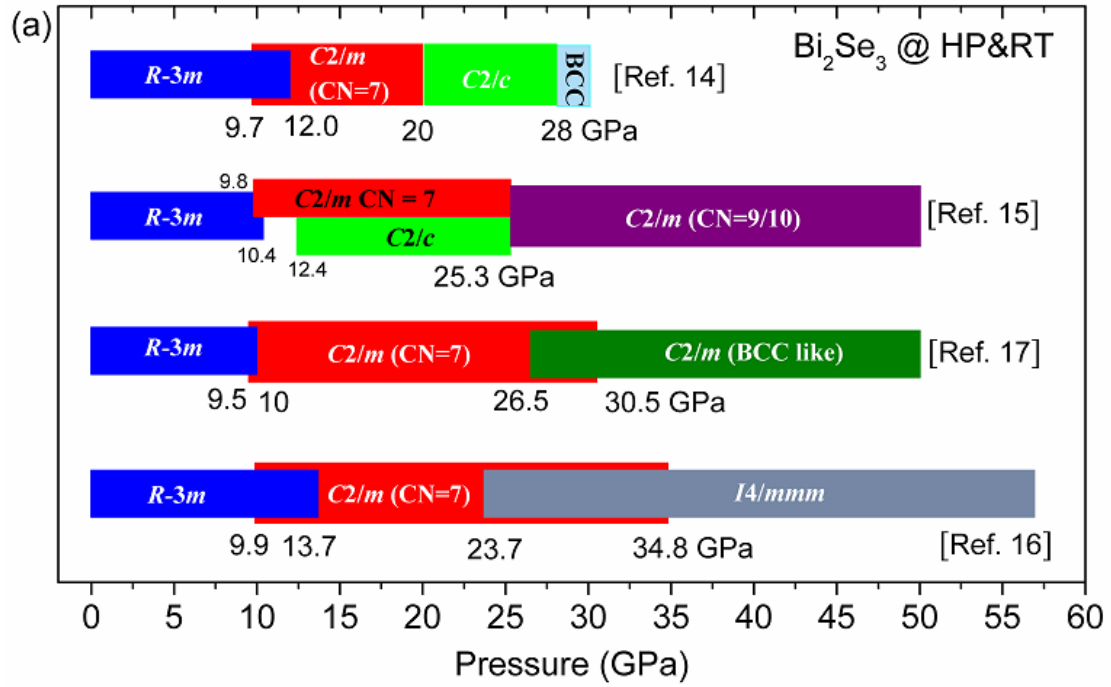


Figure 3

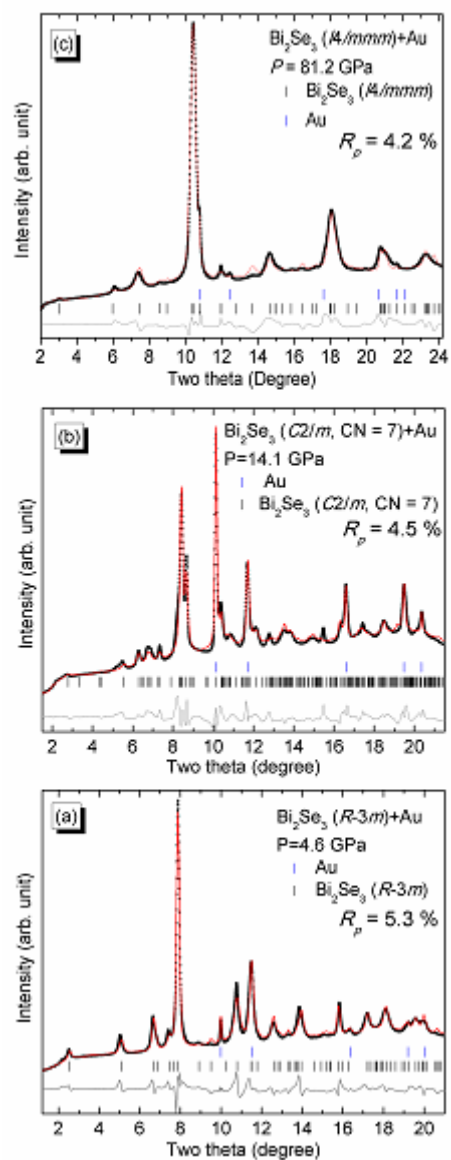


Figure 4

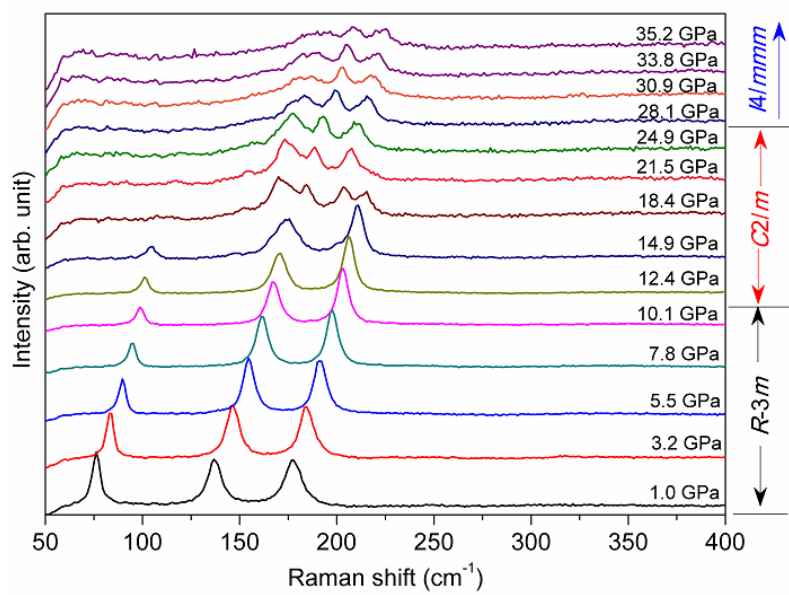


Figure 5

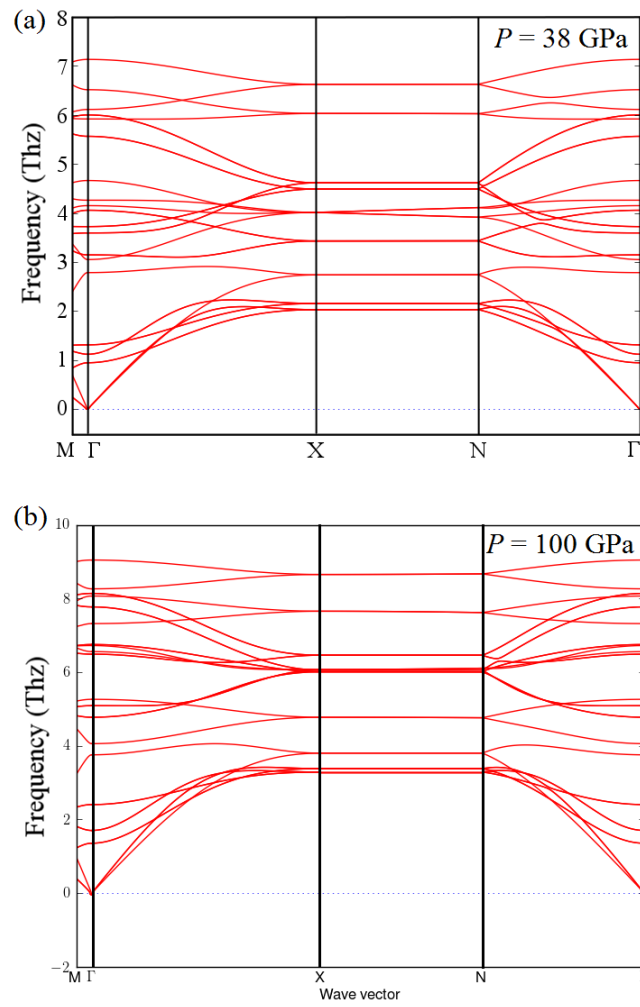
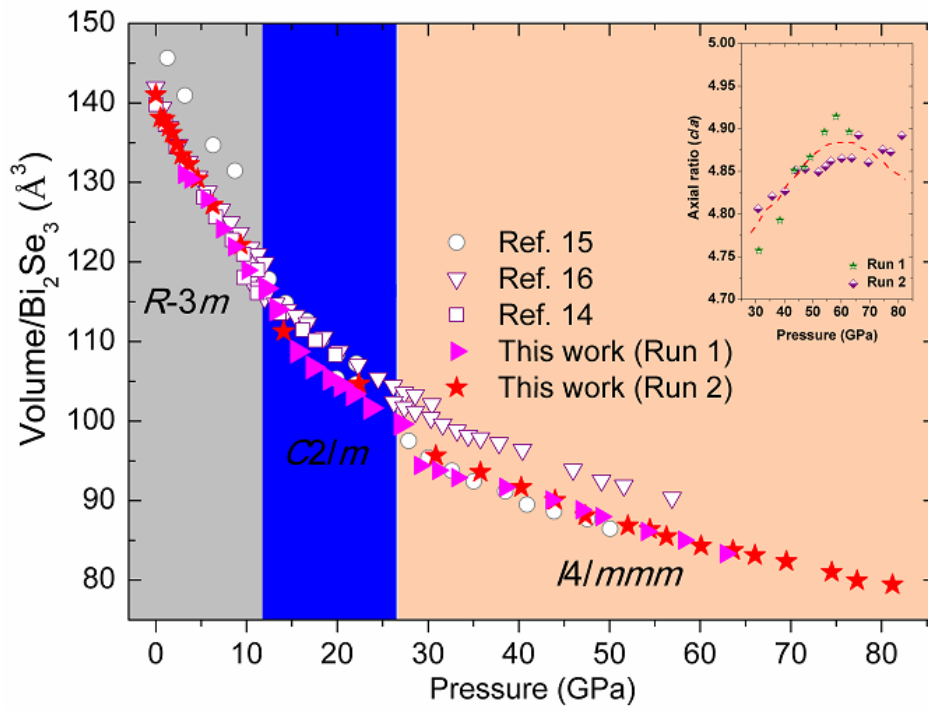


Figure 6



Acknowledgments

Portions of this work were performed at HPCAT (Sector 16), Advanced Photon Source (APS), Argonne National Laboratory. HPCAT is supported by CIW, CDAC, UNLV, and LLNL through funding from DOE-NNSA, DOE-BES, and NSF. Use of the Advanced Photon Source, an Office of Science User Facility operated for the US DOE Office of Science by Argonne National Laboratory, was supported by the US DOE under Contract No. DE-AC02-06CH11357. This work was partially supported by Natural Science Foundation of China (Grant No. 10904022). Portions of this work were performed at the BL15U1 beamline, shanghai synchrotron radiation facility (SSRF) in China. The authors would like to thank Shanghai Synchrotron Radiation Facility for use of the synchrotron radiation facilities.

Author contributions

Z.H.Y., L. W., J.G. Z., and H.K. M. were involved in the experiment design, data analysis and the drafting of the manuscript. G.D. G. synthesized the sample. S.S. and M.S. were responsible for the beamlines of 16-ID-B and 11-BM-B at Advanced Photon Source, respectively. S.Y. and K.Y. were responsible for the beamline of BL15U1 at SSRF. Q.Y. H. performed DFT calculation. All authors reviewed the manuscript.

Additional information

Competing financial interests: The authors declare no competing financial interests.

Structural phase transition in Bi_2Se_3 under high pressure

Zhenhai Yu¹, Lin Wang^{1,2,8*}, Qingyang Hu^{1,8}, Jinggeng Zhao³, Shuai Yan⁴, Ke Yang⁴, Matthew Suchome⁵, Stanislav Sinogeikin⁶, Genda Gu⁷ & Ho-kwang Mao^{1,6,8}

¹Center for High Pressure Science and Technology Advanced Research, Shanghai, 201203, People's Republic of China,

²State Key Laboratory of Superhard Materials, Jilin University, Changchun 130012, People's Republic of China,

³Natural Science Research Center, Academy of Fundamental and Interdisciplinary Sciences, Harbin Institute of Technology, Harbin 150080, People's Republic of China,

⁴Shanghai Institute of Applied Physics, Chinese Academy of Sciences, Shanghai 201203, People's Republic of China,

⁵X-ray Science Division, Advanced Photon Source, Argonne National Laboratory, Argonne, Illinois 60439, United States of America,

⁶High Pressure Collaborative Access Team, Geophysical Laboratory, Carnegie Institution of Washington, Argonne, Illinois 60439, United States of America,

⁷Condensed Matter Physics and Materials Science Department, Brookhaven National Laboratory, Upton, New York 11973, United States of America,

⁸Geophysical Laboratory, Carnegie Institution of Washington, Washington, DC 20015, United States of America,

* Corresponding author, Tel: 1(630)252-6763 (office), Fax 1(630)252-9303.

E-mail address: wanglin@hpstar.ac.cn, or lwang@carnegiescience.edu (Lin Wang).

(1) High resolution XRD pattern of Bi_2Se_3 under ambient conditions

High resolution synchrotron X-ray powder diffraction data were collected using the powder diffractometer at 11 BMB beamline of Advanced Photon Source at Argonne National Laboratory. The wavelength was set at 0.4124 Å. The wavelength was calibrated using Si 640c as a standard. The samples were finely ground and housed in glass capillaries that were continuously rotated during the measurements. Fig. S1 depicts a typical Rietveld refinement of $R\bar{3}m$ phase of Bi_2Se_3 under ambient conditions. The XRD pattern of Bi_2Se_3 at ambient conditions was indexed with a rhombohedral structure ($R\bar{3}m$, No. 166) and with hexagonal representation lattice parameters $a = 4.1408(9)$ Å, $c = 28.647(6)$ Å, and $V_0 = 425.4(2)$ Å³. The lattice parameters refined from this work are in good agreement with those from Nakajima et al. ($a = 4.143$ Å, $c = 28.636$ Å, and $V_0 = 425.673$ Å³).

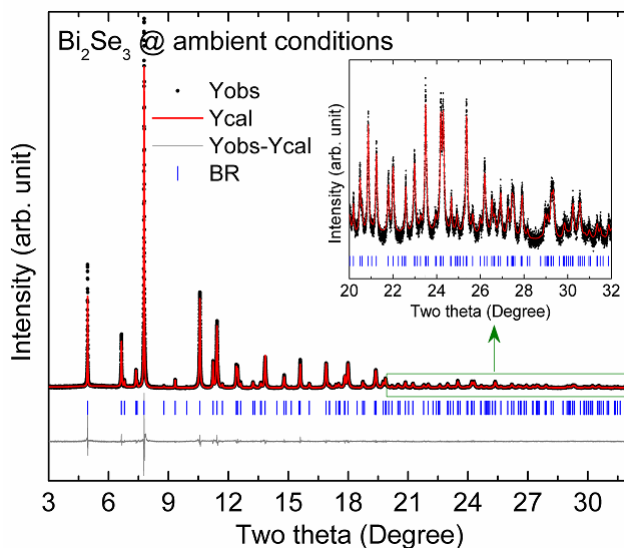


Figure S1. High resolution synchrotron X-ray diffraction profiles for Bi_2Se_3 under ambient conditions. The solid spheres are the observed data and the solid lines are the calculated diffraction patterns. The positions of the space group allowed reflections are indicated with vertical solid short lines. The inset shows the quality of the fit and data at higher angles.

(2) Angle dispersive XRD patterns of Bi_2Se_3 collected at BL15U1 beamline of Shanghai Synchrotron Radiation Facility

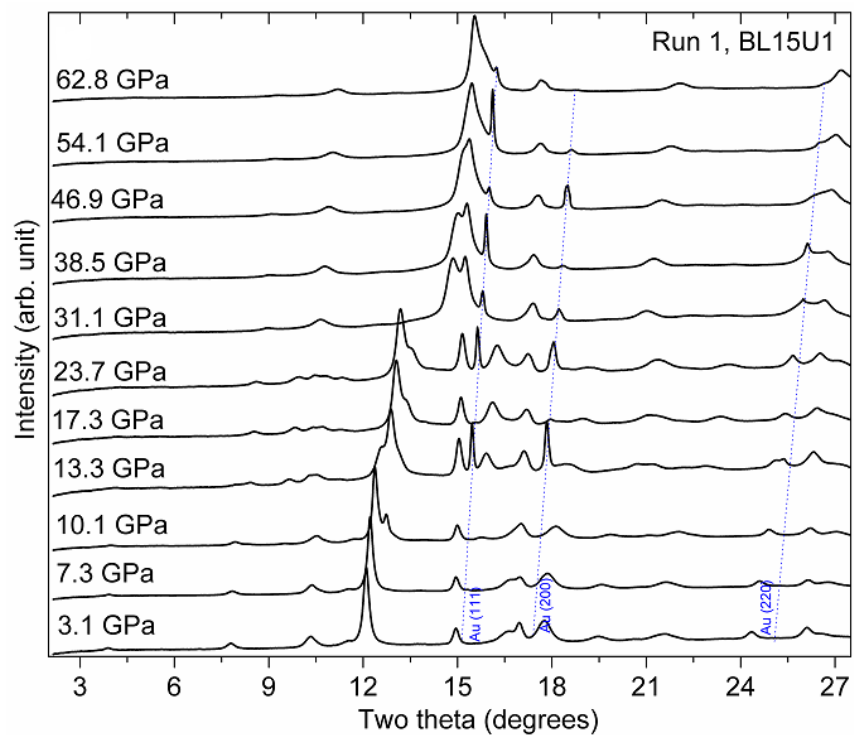


Fig. S2. Angle dispersive XRD patterns of Bi_2Se_3 under various pressures at room temperature collected at BL15U1 beamline of Shanghai Synchrotron Radiation Facility.

(3) Pressure induced electronic topological transition (ETT) in $R\text{-}3m$ phase of Bi_2Se_3

The lattice parameters a and c as a function of pressure for $R\text{-}3m$ phase of Bi_2Se_3 were obtained from the Rietveld refinement. The pressure dependence of the axial ratio (c/a) for $R\text{-}3m$ phase of Bi_2Se_3 is reported in Fig. S2. The axial ratio decrease as the pressure increase. However the slope of the axial ratio versus pressure is different. Our present measured results indicate that pressure induced ETT in Bi_2Se_3 occurred around 3 GPa. The experimentally observed pressure-induced ETT in Bi_2Se_3 was also confirmed by Vilaplana *et al.*. They observed the pressure-induced ETT in Bi_2Se_3 around 5 GPa. However the axial ratio of c/a in Vilaplana *et al.*'s results experiences minor changes among 3.4 to 8.4 GPa as shown in Fig. 3 with open symbols. A 4:1 methanol-ethanol mixture was used as PTM in Vilaplana *et al.*'s experiment [14]. No PTM was used in this work. We attribute the discrepancies to the effects of the different PTM used in the high-pressure experiments.

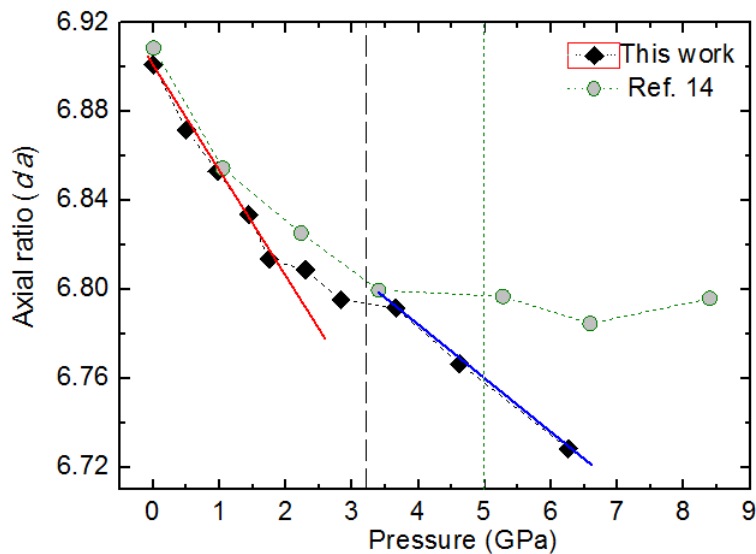


Fig. S3. The pressure dependence of axial ratio (c/a) for $R\text{-}3m$ phase of Bi_2Se_3

(4) Assignment of Wyckoff position in $C2/m$ phase of A_2B_3 -type topological insulator

Respecting the high pressure phase with space group of $C2/m$ for A_2B_3 -type topological insulator, there are three cases of assignment of Wyckoff position from the literature, (I) two types of A atoms and three types B atoms located at five nonequivalent crystallographic 4i Wyckoff position; (II) Two types of nonequivalent A atoms was situated at 4i position, the wyckoff positions for the four nonequivalent B atoms are 2a, 4i, 2c, and 4i, respectively; (III) A and B atoms could reach a state with disordered solution due to the close atomic radii of A and B atoms such as Bi, Sb and Te. The Wyckoff positions for A/B atoms are 2a and 4i, respectively.

(5) Comparison of experimental and simulated XRD patterns of Bi_2Se_3 ~ 14 GPa

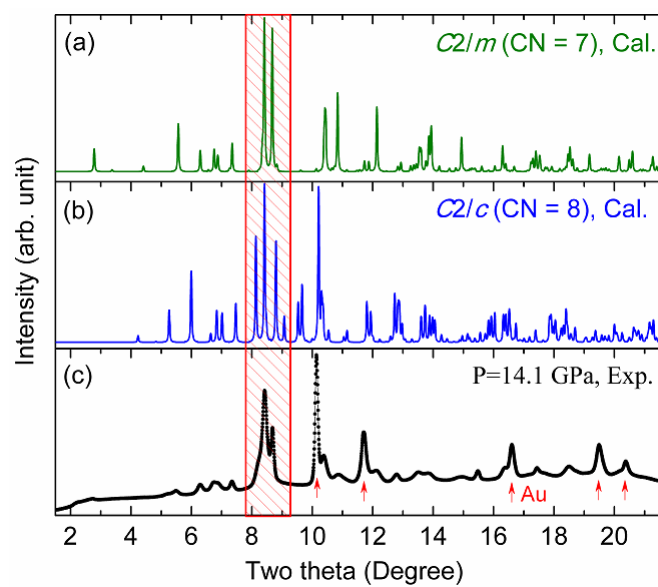


Fig. S4 Angles dispersive XRD pattern of Bi_2Se_3 ~ 14 GPa from this work (the diffraction peaks of Au were marked with red arrows) and the simulated XRD patterns with space group $C2/c$ and $C2/m$.

(6) Comparison of experimental and simulated XRD patterns of Bi_2Se_3 ~ 30 GPa

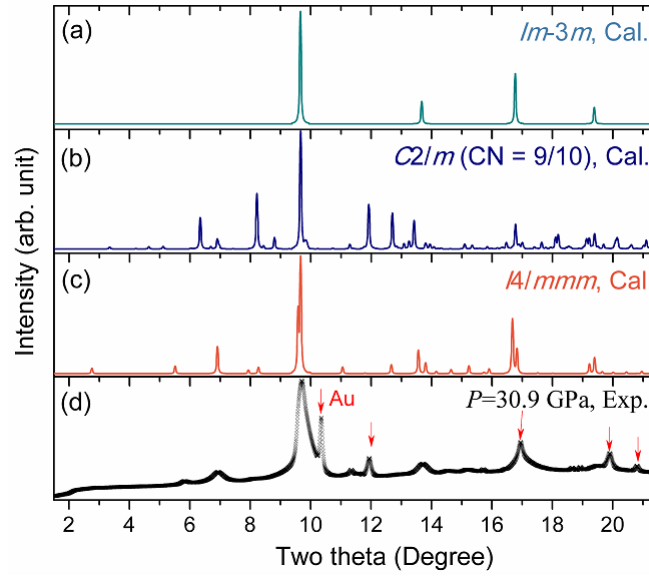


Fig. S5. The experimental and simulated XRD patterns of Bi_2Se_3 with different polymorphism under high pressure around 30 GPa. The lattice parameters of $C2/m$, $I4/mmm$ and $Im-3m$ phase of Bi_2Se_3 were referenced from Ref. (14-

17)

(7) Pressure dependence of Raman spectra of Bi_2Se_3 using no PTM (Run 2).

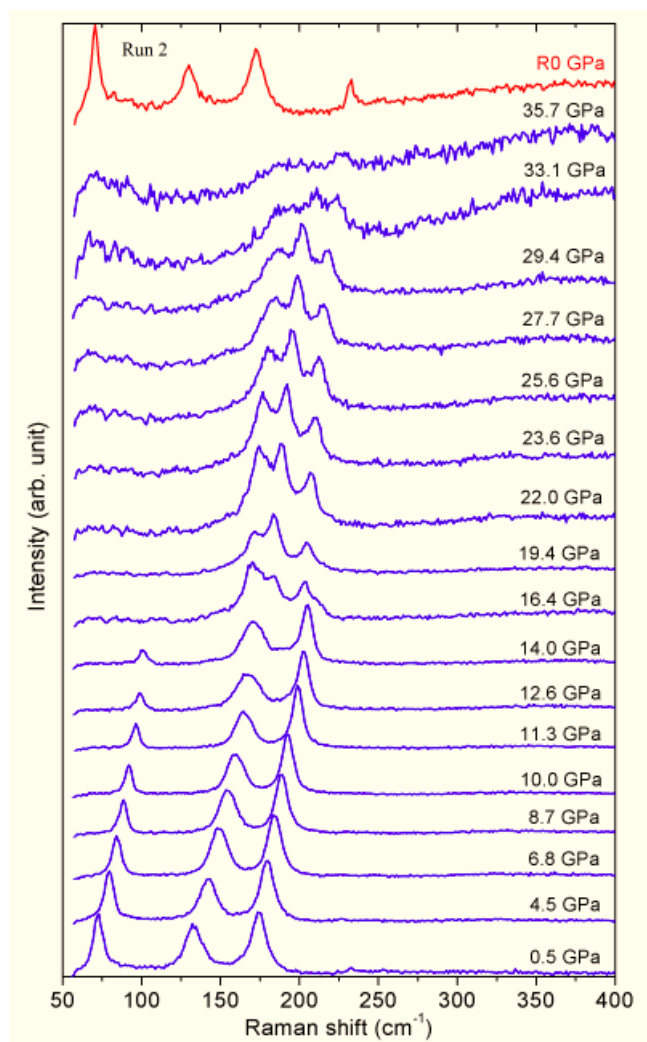


Fig. S6. Pressure dependence of Raman spectra of Bi_2Se_3 during compression and decompression (0 GPa) experimental using no PTM (Run 2).

(8) Pressure dependence of the Raman frequency and relative Raman shift of R-3m phase of Bi_2Se_3

The pressure dependence of the Raman frequencies for $R\text{-}3m$ phases of Bi_2Se_3 is reported in Fig. 6. The Raman frequency of the three observed Raman peak from two independent Runs homogeneously increase as the pressure increases for the $R\text{-}3m$ phase of Bi_2Se_3 . However, the relative Raman shift of the $R\text{-}3m$ phase of Bi_2Se_3 versus pressure is different, which is $A_{1g}^1 > E_g^2 > A_{1g}^2$. The difference between Run 1 and Run 2 lies in the profile of relative Raman shift, which come from the different hydrostatic conditions.

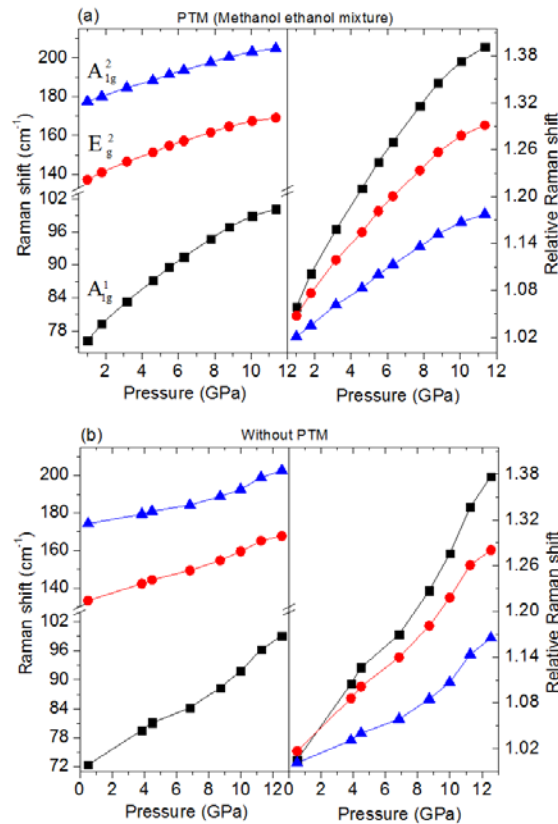


Fig. S7. Pressure dependence of the Raman frequency and relative Raman shift of R-3m phase of Bi_2Se_3 using (a) 4:1 methanol-ethanol mixture (Run 1) and (b) no PTM (Run 2).

